Inorganic Chemistry

Article

Structural Distortion-Modulated Magnetic and Dielectric Properties in Nonstoichiometric $Yb_{2−x}Ti_2O_{7−\delta}$ Pyrochlore

Ming-Yuan Yan, Xiao-Yu Zhang, Li-Huai Shu, Li-Da Chen, Jian Guo, Yu Xing, Ji Zhang, Feng-Zhen Huang, and Shan-Tao Zhang*

Cite This: *Inorg. Chem.* 2022, 61, 10425−10434

Read Online

ACCESS | Metrics & More | Article Recommendations | Supporting Information

ABSTRACT: Rare-earth titanate pyrochlores have attracted considerable attention for their unique magnetic frustration. Among those compounds, $Yb_2Ti_2O_7$, a candidate for quantum spin ice, has been extensively studied in its magnetic ground state. However, works on its dielectric property and structure-property relationship lag far more behind. Here, by preparing and investigating nonstoichiometric $Yb_{2−x}Ti_2O_{7−\delta}$ ($x = 0-0.15$) ceramics, we demonstrate that the samples with $x \leq 0.05$ maintain a single-pyrochlore phase, but the nonstoichiometry arouses significant structural distortion and increased oxygen vacancy. As a result, the ferromagnetism, indicated by a positive Curie-Weiss temperature, decreases almost linearly with increasing x value. Remarkably composition-dependent low-temperature dielectric relaxations have been observed. In addition, through introducing nonstoichiometry, the relaxor degree of dielectric behavior is enhanced, and the dielectric curve shows an altered shape. The origin of this dielectric relaxation is attributed to the increased structural distortion reflected by the changed bond length/angle, since there is no phase transition in 90−300 K. Our work gives a comprehensive view on the structural, magnetic, and dielectric properties of $Yb_2Ti_2O_7$, which is instructive for further work on pyrochlores.
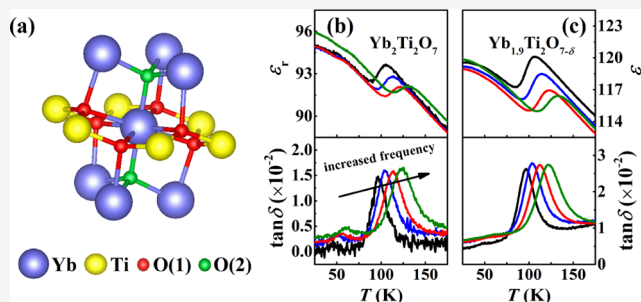
INTRODUCTION

In recent years, rare-earth titanates with pyrochlore structure have attracted considerable attention for magnetic frustration with a rich variety of unconventional ground states.[1,2] The nominal composition of these titanates is described by the chemical formula $R_2^{3+}Ti_2^{4+}O_7$, where R^{3+} is a trivalent rare-earth ion. In the cubic pyrochlore $R_2Ti_2O_7$, the arrangement of the rare-earth sublattice forms a corner-sharing tetrahedra network and leads to the geometrical frustration, and different rare-earth ions on the lattice affect the magnetic interaction.[3] Therefore, rare-earth titanate pyrochlores exhibit a wide range of exotic low-temperature magnetic states like spin ice, spin liquid, spin glass, and so on.[4−8]

Among these pyrochlore-structure titanate compounds, $Yb_2Ti_2O_7$ has been extensively studied as a candidate for quantum spin ice, and most reports focus on its magnetic ground state and related magnetic property, which, however, are still under debate.[9−11] In particular, a neutron scattering study shows evidence for an ordered low-temperature ferromagnetic state,[12] while other studies observe a dynamic disordered ground state with only short-range 3-dimensional magnetic correlations.[13−15] Moreover, theoretical description illustrates a splayed ferromagnetism with noncollinear magnetic moment, showing good agreement with experimental data.[16,17] Recently, it has been reported that the geometrical

frustration of $Yb_2Ti_2O_7$ is sensitive to the chemical disorder.[15,18,19] Therefore, to further understand the magnetic property, structurally and/or chemically modified $Yb_2Ti_2O_7$ should deserve investigations.

In addition to magnetism, pyrochlore titanate compounds are potential candidates for magneto-dielectrics or multi-ferroics since they show dielectric relaxation while some of them like $Ho_2Ti_2O_7$ and $Dy_2Ti_2O_7$ demonstrate ferroelectricity.[20−23] To find the origin of the dielectric relaxation, intense works have been done and several explanations have been proposed, including the hopping of the disordered cations at A-sites, chemical disorder, atomic displacements, etc.[24,25] Up to now, the dielectric property of $Yb_2Ti_2O_7$ has been barely reported. This means investigations on dielectric relaxation and the associated mechanism of $Yb_2Ti_2O_7$ are urgently required, which may facilitate understanding of the dielectric relaxation in rare-earth titanate pyrochlores.
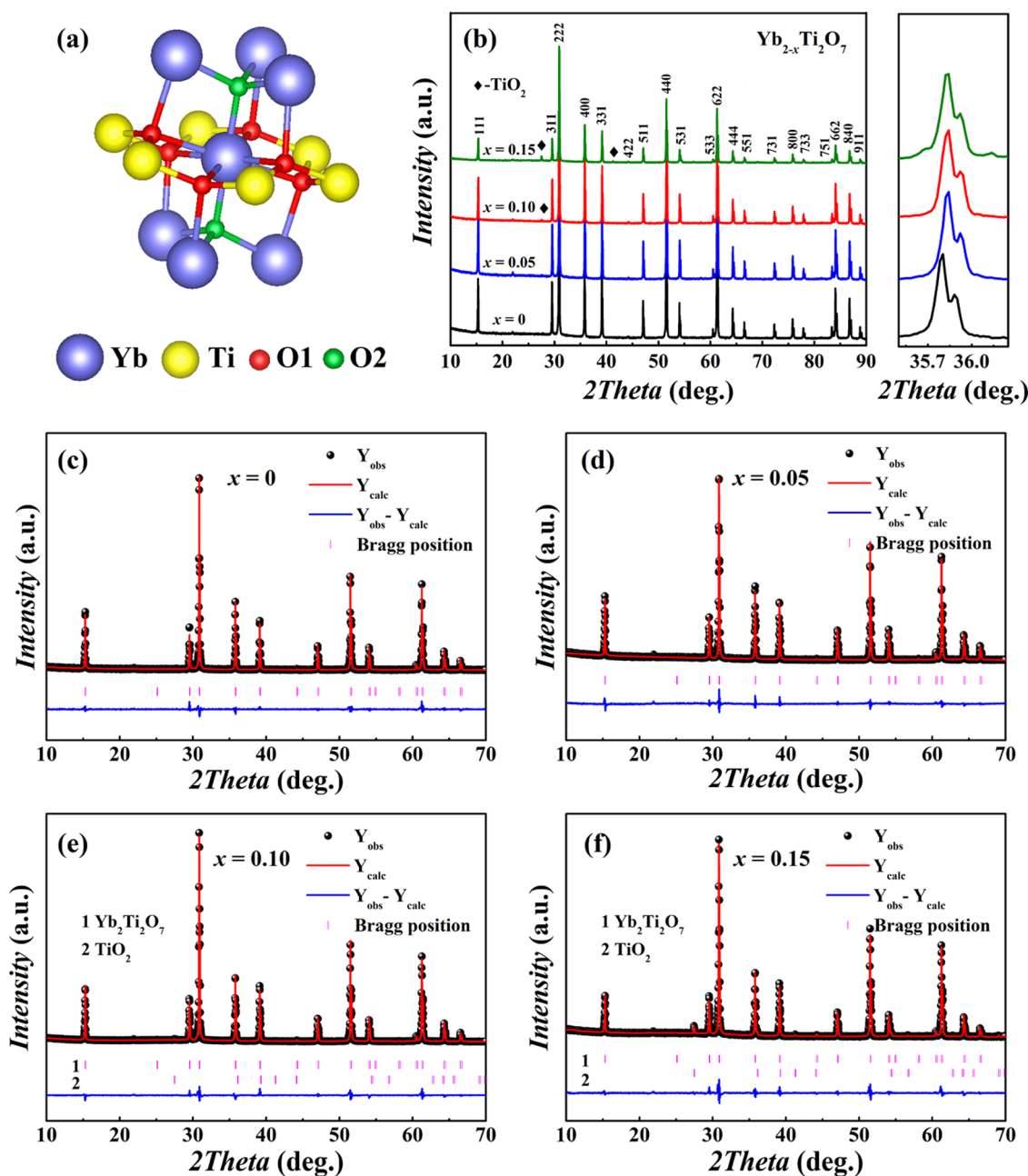
Figure 1. (a) Part of the cubic pyrochlore $Yb_{2-x}Ti_2O_{7-\delta}$. (b) X-ray diffractometer (XRD) patterns of the $Yb_{2-x}Ti_2O_{7-\delta}$ powders; the right panel shows the shifted diffraction peaks. Rietveld refinement results of (c) $x = 0$, (d) $x = 0.05$, (e) $x = 0.10$, and (f) $x = 0.15$.

A pyrochlore compound with the nominal composition of $A_2B_2O_7$ can be also expressed in the form $A_2B_2O(1)_6O(2)$, which denotes different oxygen positions in the lattice. For $Yb_2Ti_2O_7$, as shown by Figure 1a, one Yb atom is surrounded by eight oxygen atoms and one Ti atom is located in the octahedral void, which respectively occupy the Wyckoff positions of 16d and 16c. Especially, the oxygen environment around the cationic sites can be categorized into two kinds: the 48f-Wyckoff position of O(1) sites (red) and the 8b-Wyckoff position of O(2) sites (green). The O(1) atoms around the centered Yb ions are displaced in two antiparallel planar triangles, and this special occupancy of oxygen atoms could facilitate large structural distortion, which may provide a degree of freedom to modulate its properties.

Based on the above descriptions, one can see that to optimize and understand the magnetic and dielectric properties of $Yb_2Ti_2O_7$, a feasible way is to modify the structure distortion and investigate the structure-property relationship. The question is: How to modify the structure distortion? As a popular strategy in structure modulation, chemical substitution has been widely used in almost all material systems, including rare-earth titanate pyrochlores.[26] For example, the intrinsic "stuffed" nature of pyrochlore titanate in which rare-earth ions substitute the B-site Ti ions, as well as other rare-earth or nonmagnetic ions replace the A-site ions, is reported to affect the magnetic ground state.[3,18,27] However, though great achievements have been made based on chemical substitution, this method also enhances the composition's complexity, making it difficult to individually identify the contributions

from structure distortion and composition to the properties. Thus, a simple method only resulting in structure distortion may be helpful for further clarifying the structure-property relationship of pyrochlores like $Yb_2Ti_2O_7$.

In our opinion, nonstoichiometry can lead to structure distortion by modifying the bond length/bond angle without introducing composition complexity. Actually, pyrochlores have a large flexibility to tolerate nonstoichiometry without structure collapse and remain as dielectrics; thus, the as-induced point defects such as vacancies are localized. As an example, $Pb_{1.5}Nb_2O_{6.5}$ maintains a pyrochlore structure and dielectric behavior while containing several unoccupied A- and O-sites.[28,29] In addition, few previous reports have studied the structure evolution and magnetic properties of stuffed rare-earth titanates like $Yb_2Ti_2O_7$.[3,30] Therefore, it is possible to realize lattice distortion by introducing nonstoichiometry, which can further modulate the intrinsic magnetic and dielectric properties of $Yb_2Ti_2O_7$.

In this paper, we have designed and fabricated non-stoichiometric $Yb_{2-x}Ti_2O_{7-\delta}$ ($x = 0$, 0.05, 0.10, 0.15) pyrochlores, and investigated their structure-property relationship. It is found that the nonstoichiometry results in the increase of oxygen vacancy and the presence of TiO_2, leading to an enhanced lattice distortion. The ferromagnetic interaction is decreased due to the increased fraction of TiO_2 with introduction of more Yb vacancies. Moreover, a composition-dependent dielectric relaxation has been observed here, which is ascribed to the increased structural distortion.

■ EXPERIMENTAL SECTION

Polycrystalline ceramics of $Yb_{2-x}Ti_2O_{7-\delta}$ ($x = 0$, 0.05, 0.10, 0.15) were synthesized by the solid-state reaction method using Yb_2O_3 (99.99%) and TiO_2 (99%, both from Aladdin) as raw materials. The dried raw materials were weighed according to the chemical formula; each mixture was ball milled for 24 h in agate jar, dried at 80 °C for 12 h, and presintered at 1300 °C for 30 h in a high-purity alumina crucible. Then, each obtained powder was ball milled again for another 24 h, dried at 80 °C for 12 h, and calcined at 1400 °C for 30 h to obtain a single-phase powder. After the calcination, each powder was ground using an agate mortar and mixed with 7 wt % of poly(vinyl alcohol) (PVA). The reground powder was further pressed into disks with a diameter of 10 mm and a thickness of ∼1 mm. Finally, the disks were sintered at 1400 °C for 30 h and cooled down to 400 °C with a controlled cooling time of 150 min, then followed by naturally cooling down to room temperature.

The phase and crystal structure were measured by an X-ray diffractometer (XRD, Rigaku Ul-tima) with a Cu Kα1 radiation source (λ = 1.5406 Å) at 93, 200, and 300 K. The Rietveld refinements of the XRD patterns were performed by using the Fullprof Software. All patterns were refined within the space group of $Fd3m$ (No 227), which is appropriate for the rare-earth titanate pyrochlore. The occupancies of Yb^{3+} and Ti^{4+} were allowed to refine freely on 16d and 16c Wyckoff positions (Table 1) under the constraint of total occupancies on both sites maintained at nominal ratios. Moreover, anisotropic thermal factors (Debye-Waller factor) for both Yb^{3+} and Ti^{4+} ions were considered in refinements based on previous studies.[18] The oxygen thermal parameters were fixed at reasonable values due to the insensitivity of oxygen to XRD powder refinement in these heavy ion compounds.[3,30] The only free positional parameter in this structure belongs to the 48f oxygen site.

The microstructures and phase compositions of the sintered samples were analyzed via scanning electron microscopy (SEM) equipped with energy dispersive spectroscopy (EDS). Room-temperature Raman spectra were recorded using a Raman spectrometer (NR-1800, JASCO). The valence states of the constituent elements were analyzed via high-resolution X-ray photoelectron spectroscopy

Table 1. Crystallographic Sites Used in Rietveld Refinements Including Wyckoff Positions and Fractional Coordinates in the Space Group $Fd3m$

atom	Wyckoff position	fractional coordinates			ideal occ.
Yb1	16d	0.500	0.500	0.500	1
Yb2	16c	0.000	0.000	0.000	0
Ti1	16c	0.000	0.000	0.000	1
Ti2	16d	0.500	0.500	0.500	0
O1	48f	x	0.125	0.125	1
O2	8b	0.375	0.375	0.375	1

(XPS). For electrical measurements, ground disk samples with ∼0.2 mm thickness were covered by a thin layer of silver paste and fired at 500 °C for 30 min. The dielectric constant (ε_r) and dielectric loss ($\tan \delta$) were measured using an impedance analyzer (HP 4294A) at different temperatures and frequencies with and without an applied magnetic field of 1 T. The polarization−electric field ($P-E$) hysteresis curve was drawn using a precision multiferroic tester (Radiant Technologies Inc.) at 10, 77, and 300 K, while the magnetic property was measured with a superconducting quantum interference device (MPMS-3, Quantum Design).

■ RESULTS AND DISCUSSION

Figure 1b presents the room-temperature XRD patterns and partly enlarged patterns of all powder samples. As can be seen, the $x = 0$ sample has a well-crystallized pyrochlore structure with space group $Fd3m$ (JCPDS #17-0454). The diffraction peaks of the $x = 0.05$ sample are consistent with those of $x = 0$, with a still-persisting single-phase pyrochlore structure without an obvious impurity phase. However, this is not the case for the $x = 0.10$ and 0.15 samples, whose XRD patterns contain dominant diffraction peaks from the pyrochlore structure and some additional diffraction peaks from the TiO_2 secondary phase, as indicated by the symbols. On the other hand, as shown by the enlarged XRD patterns in Figure 1b, with increasing x value from 0 to 0.05, the diffraction peaks shift towards higher angles, indicating the shrinkage of the pyrochlore lattice. However, this trend does not continue to $x = 0.15$. Consistently, as shown in Figure 2, the EDS
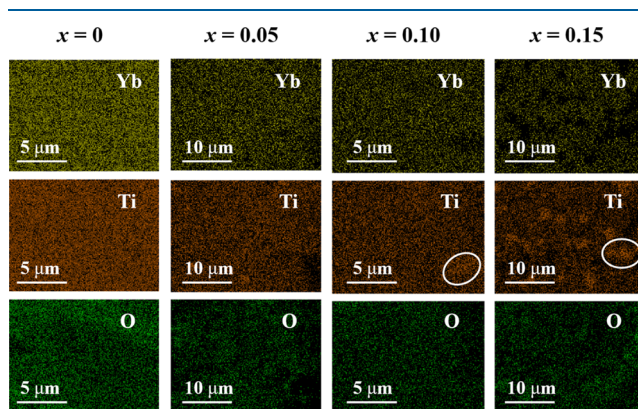
Figure 2. Elemental mapping of Yb, Ti, and O elements for $Yb_{2-x}Ti_2O_{7-\delta}$ samples.

measurements confirm that Yb, Ti, and O elements are distributed homogeneously for the $x = 0$ and 0.05 samples at the microscale, whereas the Ti element tends to be partially aggregated in the $x = 0.10$ and 0.15 samples, as shown by the marked areas. These results prove that the $Yb_{2-x}Ti_2O_{7-\delta}$ pyrochlore can tolerate ∼2.5% Yb vacancy around $x = 0.05$.

To quantitatively investigate the nonstoichiometry on the crystal structure, Rietveld refinements were carried out based on the powder XRD patterns, and the results are plotted in Figure 1c–f. The refined structural parameters for the nonstoichiometric $Yb_{2-x}Ti_2O_{7-\delta}$ are presented in Table 2.

Table 2. Basic Refined Parameters for $Yb_{2-x}Ti_2O_{7-\delta}$ Samples[a]

parameter		x			
		0	0.05	0.10	0.15
	a/Å	10.02979	10.02937	10.02934	10.03016
x pos.	48f	0.32236	0.32307	0.31941	
Yb1 occ.	16d	1.0007	0.9811	0.9558	
Yb2 occ.	16c	−0.0007	−0.0061	−0.0059	
Ti1 occ.	16d	1.0001	0.9984	0.9644	
Ti2 occ.	16c	−0.0001	0.0016	−0.0005	
	$w(P)$/%	100	100	98.97	89.62
	$w(R)$/%	0	0	1.03	10.38
	R_{wp}/%	14.8	14.4	10.2	14.6
	R_{exp}/%	10.32	7.09	3.25	6.95
	χ^2	2.05	4.13	9.81	4.39

[a] $w(P)$ and $w(R)$ refer to the mass fraction of the $Yb_2Ti_2O_7$ pyrochlore and rutile TiO_2, respectively.

The weight residuals (R_{wp}), goodness of fit (χ^2) parameters, and Debye-Waller factor (Table S1) are similar to the previously reported stuffed $Yb_2Ti_2O_7$,[3,29,30] suggesting that the structural models are reasonable to represent the modulated structure. For the stoichiometric $Yb_2Ti_2O_7$, the calculated lattice parameter a agrees well with most literature values (around 10.032 Å).[3,30] With the introduction of the Yb vacancy, a slightly decreases with $x = 0.05$, and further increases to $x = 0.15$, accompanied by the more rutile TiO_2, consistent with the EDS results shown in Figure 2. The decrease of a from $x = 0$ to 0.05 here is in agreement with the shifting of the diffraction peaks toward higher angles in the XRD patterns. The reduced magnitude of a is very close to that of the previously reported $Yb_{2+x}Ti_{2-x}O_{7-\delta}$.[30] These results indicate again that the actually tolerated Yb vacancy at the A site in the $Yb_2Ti_2O_7$ lattice is around $x = 0.05$. The low tolerance of Yb vacancy is similar to that in the reported work on stuffed $Yb_{2+x}Ti_{2-x}O_{7-\delta}$,[30] which revealed a limited composition tolerance of Yb vacancy in the $Yb_2Ti_2O_7$ pyrochlore.

Moreover, it is necessary to evaluate the composition-dependent fraction of TiO_2, which, in our opinion, is hard to be determined based on the EDS results. However, Rietveld refinements quantitatively give the fractions of TiO_2, as listed in Table 2. For the $x = 0$ and 0.05 samples, the TiO_2 fraction is zero, consistent with the XRD patterns and the uniformly distributed Ti element in the EDS mapping. Actually, the chemical compositions of both samples evaluated from EDS (Table S2) are very close to the designed nominal ones. On the other hand, the fraction of TiO_2 in the $x = 0.10$ and 0.15 samples are evaluated to be 1.03 and 10.38%, respectively, showing a similar variation trend with the XRD and EDS results.

On the other hand, the oxygen distortion can be reflected by the positional parameter x of the 48f oxygen site. For

pyrochlore oxides, the positional parameter x usually lies in the range 0.320−0.345, whereas the positional parameter $x = 0.3125$ shows a perfect octahedron around the 16c site. Here, the refined values of the positional parameter x around 0.320 indicate again the pyrochlore structure of $Yb_{2-x}Ti_2O_{7-\delta}$ with a distorted oxygen octahedron. In addition to this, previous reports have studied the structure evolution of stuffed rare-earth titanates like $Yb_2Ti_2O_7$.[3,18,30] However, in our case of pristine $Yb_2Ti_2O_7$, the refined occupancies of Yb on the Ti site and Ti on the Yb site are very close to zero, indicating no "stuffing" effect. This observation is also consistent with the results reported in sintered powder by Rosss and Lau.[3,18] With Yb vacancy increasing to 0.05 and 0.10, the occupancy of Ti on the Yb site is still negligible.

Raman spectroscopy has been extensively used to analyze the structural information concerning local disorder in the pyrochlore structures. As can be seen from Figure 3, two
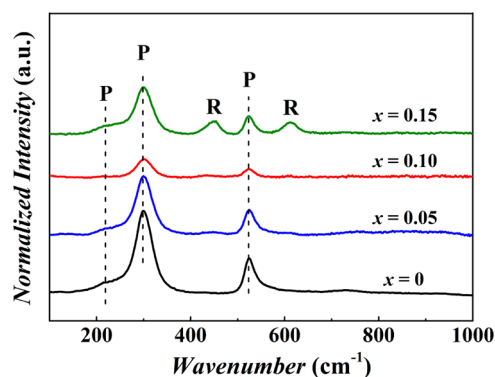

Figure 3. Normalized Raman spectra of the $Yb_{2-x}Ti_2O_{7-\delta}$ samples with $x = 0$, 0.05, 0.10, and 0.15. R: rutile TiO_2, P: pyrochlore.

additional Raman bands around 450 and 614 cm^{-1} attributed to the rutile TiO_2 are observed for $x = 0.15$.[31] Likewise, the weak peaks of TiO_2 are also found in the $x = 0.05$ and 0.10 samples. This analysis is consistent with the existence of TiO_2 indicated by the XRD patterns for $x = 0.10$ and 0.15 (Figure 1b). However, the presence of TiO_2 in $x = 0.05$ suggests that the Raman technique is highly sensitive to trace impurities, which were not detected by XRD. This result further indicates that the tolerance of Yb vacancy in the $Yb_2Ti_2O_7$ pyrochlore is close to 2.5%, consistent with the above discussion based on the XRD and EDS results.

In addition, the vibrational modes of the chemical bonds in the $Yb_{2-x}Ti_2O_{7-\delta}$ samples are obtained using Raman spectroscopy. Theoretically, the two different oxygen sites allow three types of chemical bonds, i.e., Yb−O(1) bond, Ti−O(1) bond, and Yb−O(2), which contribute to different Raman vibrational modes.[32] Moreover, according to the group theoretical analysis, an ideal cubic pyrochlore structure would yield six Raman active modes, expressed as $\Gamma_{opt} = A_{1g} + E_g + 4F_{2g}$, which are associated with the movement of oxygen atoms.[32] As one can see, three bands near 212, 302, and 525 cm^{-1} are detected for all samples. The Raman band near 302 cm^{-1} is identified as the F_{2g} mode, which is related to the bending and stretching vibrations of the Yb−O(1), Yb−O(2), and Ti−O(1) bonds.[33] The Raman mode near 525 cm^{-1} is assigned to A_{1g}, which is predominantly caused by the bending vibration of the TiO_6 octahedra.[33] The band at 212 cm^{-1} is attributed to a disorder-induced Raman active mode caused by the vibration of Ti−O(1) bonds.[34] Notably, the E_g Raman mode can be
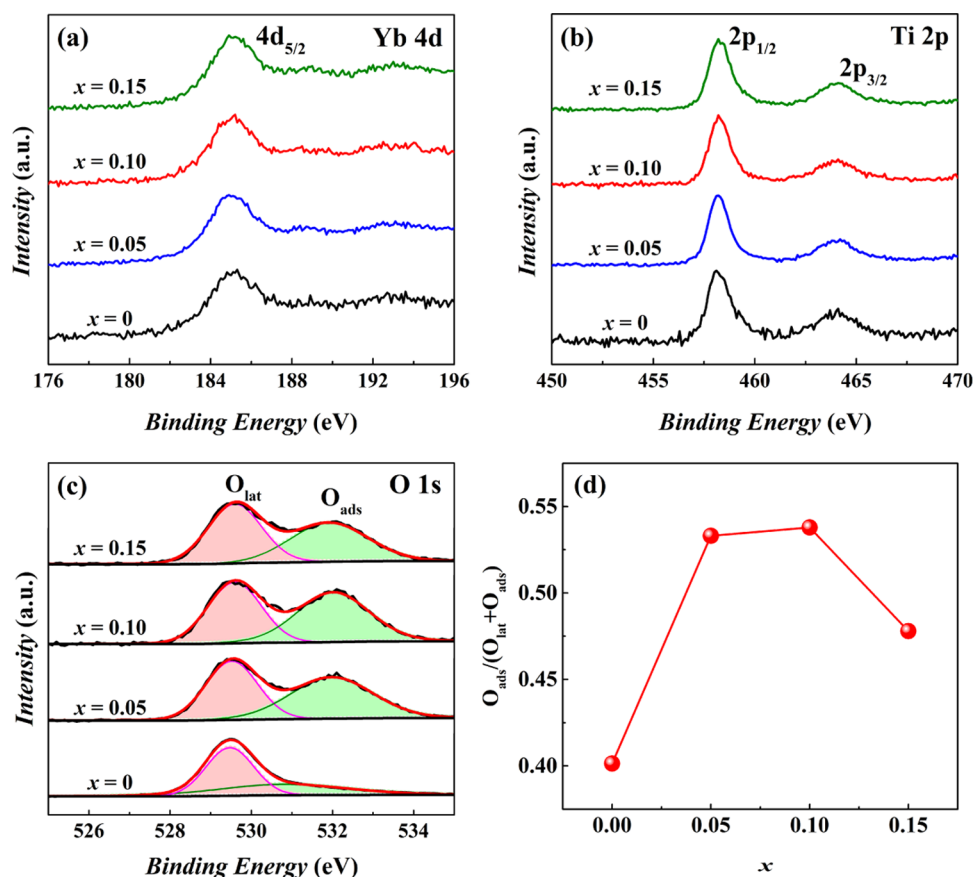
Figure 4. XPS spectra of (a) Yb 4d, (b) Ti 2p, and (c) O 1s spectra of the $Yb_{2-x}Ti_2O_{7-\delta}$ samples. (d) Relative ratio of adsorbed oxygen $O_{ads}/$ (lattice oxygen O_{lat} + adsorbed oxygen O_{ads}) as a function of the Yb vacancy.
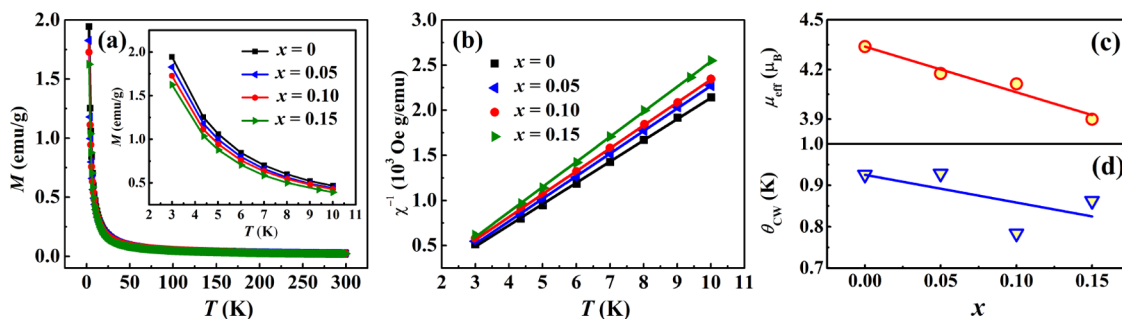
Figure 5. (a) Magnetization-temperature ($M-T$) curves of $Yb_{2-x}Ti_2O_{7-\delta}$ powder samples; the inset shows the $M-T$ curves at 3−10 K. (b) Temperature-dependent inverse susceptibility at 3−10 K; the solid lines are fitted based on Curie-Weiss law. (c) Effective moment (μ_{eff}) and (d) Curie-Weiss temperature (θ_{CW}) extracted from the measured data at 3−10 K.

hardly observed here. Generally speaking, the intensity of a Raman mode directly depends on the number of corresponding bonds.[35] As shown by Figure 3, the intensities of Raman spectroscopy for different samples have been normalized by dividing all Raman bands by a constant, and the normalized intensities of F_{2g} and A_{1g} modes decrease drastically with increasing Yb vacancy, which provides further evidence for the increased degree of structural disorder.

To investigate the effects of the introduced Yb vacancy on the chemical valence states, a detailed XPS analysis is carried out on the constituent elements Yb, Ti, and O. All recorded data have been calibrated according to the C 1s peak at 284.8 eV. Figure 4a depicts the core-level XPS spectra of Yb $4d_{5/2}$ of the $Yb_{2-x}Ti_2O_{7-\delta}$ samples, from which it can be seen that the

binding energy peak is located at 185.0 eV, showing a typical signature of Yb^{3+}, and there are no peaks at 181.0 eV corresponding to Yb^{2+}.[36] Likewise, the core-level XPS spectra of Ti 2p are presented in Figure 4b. The binding energies of the two distinct peaks at 458.8 and 464.0 eV belong to Ti $2p_{1/2}$ and Ti $2p_{3/2}$ states, respectively, and both peaks are symmetric, indicating the chemical state of Ti^{4+}.[36] These results demonstrate that the nonstoichiometry of the Yb vacancy can hardly affect the valence states of Yb and Ti ions.

Intriguingly, as the Yb vacancy content changes, the O 1s signals exhibit a different shape, as shown in Figure 4c. To further analyze this variation behavior, the XPS spectra of O 1s are fitted through two peaks by Gaussian-Lorentzian fitting. The peak at the lower binding energy (529.0 eV) can be

assigned to the lattice oxygen (O_{lat}), and the other peak at 532.0 eV can be attributed to the adsorbed oxygen (O_{ads}). It is reported that the number of oxygen vacancies can be estimated from the relative proportion of adsorbed oxygen on the XPS fitting.[37,38] Therefore, the relative ratios of $O_{ads}/(O_{lat} + O_{ads})$ were calculated and are plotted in Figure 4d. Apparently, on increasing the Yb vacancy to $x = 0.05$, the $O_{ads}/(O_{lat} + O_{ads})$ ratio increases, illustrating the growing oxygen vacancy concentration. This can be understood by the charge balance in the system as the Yb content decreases, while the Yb and Ti ions keep constant valence states of +3 and +4, respectively. As described above, the stuffing effect is excluded by Rietveld refinements; therefore, this result further supports that the increased oxygen vacancy results from the Yb vacancy. However, the oxygen vacancy content slightly increases for $x = 0.10$ and even declines for $x = 0.15$. Considering the composition-dependent TiO_2 impurity phase content derived from Rietveld refinements, the oxygen vacancy content should be negatively related with the presence of the TiO_2 impurity phase. This also supports that the tolerance limit of the Yb vacancy in the pyrochlore structure is around 2.5%. The introduction of the Yb vacancy will cause lattice distortion and elevate the oxygen vacancy content, which is reasonable to influence the magnetic and dielectric properties, as will be discussed below.

Figure 5a illustrates the temperature dependence of the magnetization curves ($M-T$) of the $Yb_{2-x}Ti_2O_{7-\delta}$ powders measured under a magnetic field of 1000 Oe. Notably, there is no significant difference in data obtained from zero-field cooling (ZFC) and field cooling (FC) measurements, with typical results of $x = 0$ plotted in Figure S1, and thus, only FC $M-T$ curves are presented here. For all samples, the magnetization decreases dramatically from 3 to 50 K and gradually reduces to zero on increasing the temperature to 300 K. This indicates that no long-range magnetic ordering transition occurs down to 3 K.[39,40] On the other hand, the magnetization decreases with increasing Yb vacancy, as shown by the inset in Figure 5a. Figure 5b plots the temperature (3–10 K)-dependent inverse susceptibility χ^{-1}, consistent with the adopted low-temperature range in previous studies for Curie-Weiss (CW) fits due to the lowest crystal-field excitation.[3,30] The solid line shows the theoretical value calculated based on the CW law,[39] expressed as eq 1

$$\chi = \frac{N_A \mu_{eff}^2}{3k_B(T - \theta_{CW})} \tag{1}$$

where N_A is the Avogadro number, k_B is the Boltzmann constant, θ_{CW} is the Curie-Weiss temperature, and μ_{eff} is the effective magnetic moment. As shown in Figure 5b, the low-temperature experimental data agrees well with the theoretical line. The values of θ_{CW} and μ_{eff} were also obtained from eq 1, as plotted in Figure 5c,d. It is to be noted that the calculated θ_{CW} (~ 0.92 K) for the $x = 0$ sample is close to the reported value for $Yb_2Ti_2O_7$,[41] and the positive θ_{CW} affirms the weak ferromagnetic interaction. Likewise, the obtained μ_{eff} (~ 4.34 μ_B) for $x = 0$ is close to the free ion moment, $\mu = 4.54$ μ_B, of Yb^{3+}, which is calculated by the equation $\mu_{eff} = g\sqrt{J(J+1)} = 4.54\mu_B$, where $g = 8/7$ is the Landau factor and $J = 7/2$ is the corresponding quantum number for Yb^{3+}.[42] Moreover, both θ_{CW} and μ_{eff} decrease with increasing Yb vacancy, indicating the decreased ferromagnetic coupling. The variation trend of μ_{eff} here is different from the rough

constant μ_{eff} in the reported $Yb_{2+x}Ti_{2-x}O_{7-\delta}$ system,[30] which is mainly due to the increased fraction of the TiO_2 impurity phase, as shown by the Rietveld refinements.

The magnetic field-dependent magnetization ($M-H$) curves of the $x = 0$ sample measured at different temperatures are presented in Figure 6a, and those of the $x = 0.05$, 0.10, and
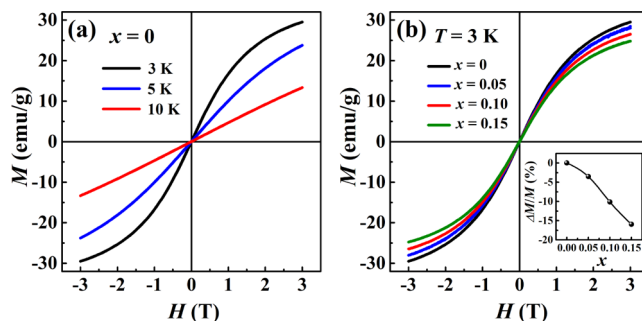
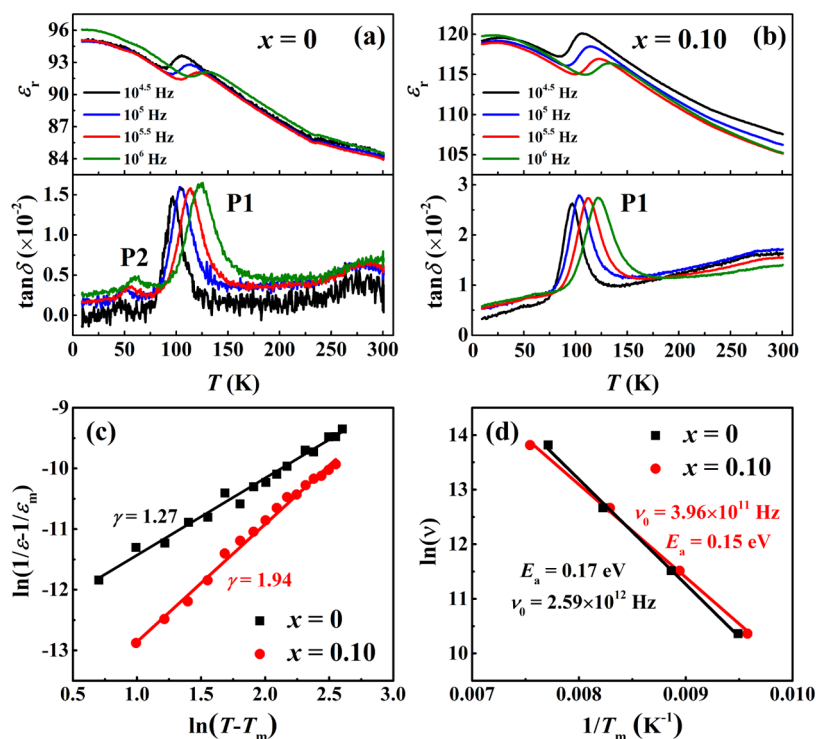**Figure 6.** (a) $M-H$ curves of the $x = 0$ sample measured at different temperatures. (b) Composition-dependent $M-H$ curves of $Yb_{2-x}Ti_2O_{7-\delta}$ samples measured at 3 K; the inset shows the corresponding reduced magnitude of magnetization as a function of x.

0.15 samples are shown in Figure S2. For each sample, the $M-H$ curve tends to saturate with increasing magnetic field up to $H = 3$ T at the lowest measuring temperature, $T = 3$ K. However, the saturation tendency weakens with increasing measuring temperature, e.g., the $M-H$ curve measured at 10 K seems to be linear up to $H = 3$ T. In general, such a temperature-dependent $M-H$ is comparable to that of the reported $Yb_2Ti_2O_7$.[41]

Figure 6b displays the composition-dependent $M-H$ curves measured at $T = 3$ K. Clearly, the maximum magnetization decreases with increasing Yb vacancy content, consistent with the reduced effective magnetic moment (Figure 5c). To analyze the composition dependence of magnetization, the reduced magnitude of magnetization $\Delta M/M$ is defined as $\Delta M/M = [M(x) - M(0)]/M(0)$, where $M(x)$ and $M(0)$ are the maximum magnetization of the sample with and without the Yb vacancy, respectively. The variation trend of $\Delta M/M$ versus x is plotted in the inset of Figure 6b. One can see that the $\Delta M/M$ value decreases almost linearly with increasing x, reaching a maximum of 16% at $x = 0.15$.

Temperature-dependent dielectric constant ($\varepsilon_r - T$) and dielectric loss ($\tan\delta - T$) curves of the disk samples were measured with different frequencies, and the results of the $x = 0$ and 0.10 samples are comparatively illustrated in Figure 7a,b. There are two important features worthy to be emphasized. First, the maximum dielectric constant ($\varepsilon_{r,max}$) decreases while the temperature (T_{max}) corresponding to $\varepsilon_{r,max}$ increases with increasing frequency. This feature represents a typical dielectric relaxation nature, which is significantly different from the rarely reported dielectric behavior of the $Yb_2Ti_2O_7$ system.[43] To identify the relaxor degree, the critical exponent γ is calculated based on the data collected at $10^{4.5}$ Hz by using eq 2, and the results are shown in Figure 7c. In particular, the γ is 1.27 for $x = 0$ while it is 1.94 for $x = 0.10$. Considering that $\gamma = 1$ for an ideal non-relaxor behavior and $\gamma = 2$ for an ideal relaxor behavior,[44] these results confirm that both samples are relaxor dielectrics and Yb vacancy enhances the relaxor degree.

$$1/\varepsilon - 1/\varepsilon_{r,max} = (T - T_{max})^\gamma / C \tag{2}$$

Figure 7. $\varepsilon_r - T$ and $\tan\delta - T$ curves of the (a) $x = 0$ and (b) $x = 0.10$ samples. The plots of (c) $\ln(1/\varepsilon_r - 1/\varepsilon_m)$-$\ln(T - T_m)$ and (d) $\ln(\nu) - 1/T_m$ of the $x = 0$ and 0.10 samples.

Second, under the measured frequency of $10^{4.5}$ Hz, the $\varepsilon_r - T$ curve of the $x = 0$ sample shows two successive dielectric relaxation peaks, P1 around 104 K and P2 around 50 K, respectively, which are obviously reflected in the $\tan\delta - T$ curve. This behavior resembles the dielectric relaxation reported in $Ho_2Ti_2O_7$ and $Dy_2Ti_2O_7$.[45] However, for the $x = 0.10$ sample, the $\varepsilon_r - T$ and $\tan\delta - T$ curves only exhibit one obvious peak at 107 K with the same measured frequency. This indicates that the nonstoichiometry-introduced Yb vacancy suppresses the dielectric relaxation peak P2, and slightly drives the dielectric relaxation peak P1 to a higher temperature. Moreover, the values of ε_r and $\tan\delta$ near P1 are enhanced with the increased Yb vacancy. For example, the ε_r values for $x = 0$ and 0.10 are, respectively, 93.6 and 120.1 under the frequency of $10^{4.5}$ Hz. The increase of ε_r and $\tan\delta$ possibly originates from the increased structural defects and distortion due to the introduction of the Yb vacancy, in good agreement with the previous study.[46]

To explain the origin of the observed dielectric relaxation, the possibility of phase transition is explored by temperature-dependent XRD performed on the $x = 0$ sample. As shown in Figure S3, the diffraction peaks of the XRD patterns measured at 93, 200, and 300 K show a clear pyrochlore structure, and do not reveal the temperature-driven structure transition. Besides, the polarization as a function of the electric field ($P-E$) curves obtained at 10, 77, and 300 K does not exhibit any hysteresis behavior (Figure S4). Therefore, the existence of a ferroelectric phase transition can be safely excluded, which is consistent with the previous neutron diffraction study on $Yb_2Ti_2O_7$.[18] Hence, the observed dielectric relaxation and its composition dependence should be ascribed to the structural distortion.

For confirmation, the activation energy (E_a) and the characteristic frequency (ν_0) of dielectric relaxations were fitted based on the Arrhenius equation:[24]

$$\nu_r = \nu_0 \exp\left(\frac{-E_a}{k_B T_{max}}\right) \tag{3}$$

where ν_r is the frequency used for dielectric measurement and k_B is the Boltzmann constant. The plot of $\ln\nu_r$ vs $1/T_{max}$ is given in Figure 7d, exhibiting a good linear fit. For the dielectric relaxation near 100 K, the obtained E_a and ν_0 are 0.17 eV and 2.59×10^{12} Hz for the $x = 0$ sample, while they are 0.15 eV and 3.96×10^{11} Hz for the $x = 0.10$ sample. Both E_a and ν_0 values are close to those of other reported dielectric pyrochlores.[47] Especially, the ν_0 values here are around 10^{12} Hz, lying in the range of $10^{10}-10^{14}$ Hz, suggesting that the dielectric relaxation is inherently involved in the polar lattice vibrational effects caused by the local distortions.[45] Notably, the inherent lattice distortion for $Yb_2Ti_2O_7$ is reflected by the fact that the refined positional parameter x value of around 0.320 (Table 2) deviates from $x = 0.3125$ with a perfect octahedron around the 16c site, which leads to the dielectric relaxation.

Normally, the dielectric relaxation of $A_2B_2O(1)_6O(2)$ pyrochlores is believed to be generated by the local structural distortion related to oxygen positions, and influenced by the phonon branches with $O(1)-A-O(1)$ and $O(2)-A-O(2)$ bending modes.[48] Compared with the activation energy and assigned phonon modes, a conclusion could be drawn that the dielectric relaxation near 100 K originates from the local lattice distortion caused by $O(1)$ oxygen sites, which would be affected by the $O(1)-A-O(1)$ bending mode-induced phonon branches, while the dielectric relaxation near 50 K can be explained by the structural distortion with $O(2)$ oxygen sites and corresponding $O(2)-A-O(2)$ bending modes. Thus,

Table 3. Values of Lattice Constant, Bond Length, and Bond Angle Obtained from Rietveld Refinements

$Yb_{2-x}Ti_2O_{7-\delta}$	bond length (Å)			bond angle (deg)		
	Yb−O(1)	Yb−O(2)	Ti−O(1)	O(1)−Yb−O(1)	O(2)−Yb−O(2)	O(1)−Ti−O(1)
$x = 0$	2.514(9)	2.17145(4)	1.916(5)	62.72(2)	180	86.1(5)
$x = 0.05$	2.551(7)	2.17141(4)	1.896(4)	62.28(8)	180	88.2(4)
$x = 0.10$	2.549(5)	2.17140(0)	1.898(1)	62.31(3)	180	88.0(1)

the change of composition at the A-site-induced structure distortion would affect both bending modes and further dielectric relaxations.

In our cases, by varying the A-site Yb vacancy content, the bond lengths of Yb/Ti−O(1) and Yb−O(2), as well as the bond angle of O(1)−Yb/Ti−O(1) are affected (Table 3), suggesting the increased lattice distortion, consistent with the Raman results. Moreover, the presence of TiO_2 may further enhance this distortion. Accordingly, the dielectric response of $x = 0.10$ alters its shape compared with that of $x = 0$: that is, the disappeared peak P2 and the slightly shifted dielectric relaxation peak P1. Moreover, the characteristic frequency values (ν_0) for the dielectric relaxation near 100 K are significantly different in the $x = 0$ and 0.10 samples. Therefore, the introduction of the A-site Yb vacancy indeed influences the dielectric relaxation behaviors of $Yb_2Ti_2O_7$, which originate from the structure distortion related to both O(1) and O(2) oxygen sites.

To reveal the magneto-dielectric response, the temperature-dependent dielectric constants of the $x = 0$ and 0.10 samples were measured with 1 T magnetic field, and the $\varepsilon_r − T$ curves under different frequencies are plotted in Figure S5. The measured results of the dielectric constant at 10^5 Hz are comparatively depicted in Figure 8. One can see that for
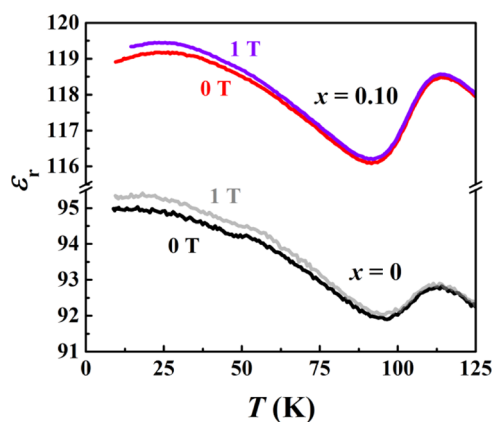

Figure 8. Temperature-dependent dielectric constant of the $x = 0$ and 0.10 samples with and without the 1 T magnetic field.

temperatures lower than 100 K, the dielectric constants of the $x = 0$ sample measured with and without magnetic field show an obvious discrepancy (Figures 7, S5, and 8), exhibiting a magneto-dielectric response. A similar magneto-dielectric effect has been reported for the $Dy_2Ti_2O_7$ single crystal.[23] Moreover, with increasing Yb vacancy from $x = 0$ to 0.10, the temperature at which the magneto-dielectric response occurs changes from 100 to 60 K, illustrating a composition-dependent behavior. The explanation for this phenomenon may be that the suppressed magnetization (Figures 5 and 6) weakens the coupling between the dielectric and magnetic properties.

CONCLUSIONS

We have investigated the crystal structure, and magnetic and dielectric properties of the $Yb_{2-x}Ti_2O_{7-\delta}$ pyrochlore with $x = 0$, 0.05, 0.10, and 0.15. The introduction of Yb vacancy leads to the lattice distortion, which not only weakens the ferromagnetic interaction but also leads to remarkably composition-dependent dielectric relaxations. Moreover, a magneto-dielectric response is observed. These results are helpful to comprehensively understand the structure-property relationship of pyrochlore titanates.

ASSOCIATED CONTENT

Supporting Information

The Supporting Information is available free of charge at https://pubs.acs.org/doi/10.1021/acs.inorgchem.2c01208.

Anisotropic thermal factors, the normalized ratio of Yb, Ti, and O elements, ZFC and FC $M−T$ curves, $M−H$ curves, low-temperatures XRD patterns and $P−E$ curves, and dielectric constant $(\varepsilon_r−T)$ as well as dielectric loss $(\tan \delta−T)$ curves measured under a magnetic field of 1 T (PDF)

AUTHOR INFORMATION

Corresponding Author

Shan-Tao Zhang − National Laboratory of Solid State Microstructures, College of Engineering and Applied Science & Jiangsu Key Laboratory of Artificial Functional Materials & Collaborative Innovation Center of Advanced Microstructures, Nanjing University, Nanjing 210093, China; orcid.org/0000-0002-6291-0363; Email: stzhang@nju.edu.cn

Authors

Ming-Yuan Yan − National Laboratory of Solid State Microstructures, College of Engineering and Applied Science & Jiangsu Key Laboratory of Artificial Functional Materials & Collaborative Innovation Center of Advanced Microstructures, Nanjing University, Nanjing 210093, China

Xiao-Yu Zhang − National Laboratory of Solid State Microstructures, College of Engineering and Applied Science & Jiangsu Key Laboratory of Artificial Functional Materials & Collaborative Innovation Center of Advanced Microstructures, Nanjing University, Nanjing 210093, China

Li-Huai Shu − National Laboratory of Solid State Microstructures and Physics School, Nanjing University, Nanjing 210093, China

Li-Da Chen − National Laboratory of Solid State Microstructures, College of Engineering and Applied Science & Jiangsu Key Laboratory of Artificial Functional Materials & Collaborative Innovation Center of Advanced Microstructures, Nanjing University, Nanjing 210093, China

Jian Guo − National Laboratory of Solid State Microstructures, College of Engineering and Applied Science & Jiangsu Key Laboratory of Artificial Functional Materials

    & *Collaborative Innovation Center of Advanced Microstructures, Nanjing University, Nanjing 210093, China*

Yu Xing − *School of Physics, Southeast University, Nanjing 211189, China*

Ji Zhang − *School of Materials Science and Engineering, Nanjing University of Science and Technology, Nanjing 210094, China;* ⊙ orcid.org/0000-0001-5447-6301

Feng-Zhen Huang − *National Laboratory of Solid State Microstructures and Physics School, Nanjing University, Nanjing 210093, China*

Complete contact information is available at:
https://pubs.acs.org/10.1021/acs.inorgchem.2c01208

Author Contributions

The manuscript was written through the contributions of all authors. All authors have given approval to the final version of the manuscript.

Notes

The authors declare no competing financial interest.

◼ REFERENCES

(1) D'Ortenzio, R. M.; Dabkowska, H. A.; Dunsiger, S. R.; Gaulin, B. D.; Gingras, M. J. P.; Goko, T.; Kycia, J. B.; Liu, L.; Medina, T.; Munsie, T. J.; Pomaranski, D.; Ross, K. A.; Uemura, Y. J.; Williams, T. J.; Luke, G. M. Unconventional magnetic ground state in $Yb_2Ti_2O_7$. *Phys. Rev. B* **2013**, *88*, No. 134428.

(2) Scheie, A.; Kindervater, J.; Säubert, S.; Duvinage, C.; Pfleiderer, C.; Changlani, H. J.; Zhang, S.; Harriger, L.; Arpino, K.; Koohpayeh, S. M.; Tchernyshyov, O.; Broholm, C. Reentrant Phase Diagram of $Yb_2Ti_2O_7$ in a <111> Magnetic Field. *Phys. Rev. Lett.* **2017**, *119*, No. 127201.

(3) Lau, G. C.; Muegge, B. D.; McQueen, T. M.; Duncan, E. L.; Cava, R. J. Stuffed rare earth pyrochlore solid solutions. *J. Solid State Chem.* **2006**, *179*, 3126−3135.

(4) Morris, D. J. P.; Tennant, D. A.; Grigera, S. A.; Klemke, B.; Castelnovo, C.; Moessner, R.; Czternasty, C.; Meissner, M.; Rule, K. C.; Hoffmann, J. U.; Kiefer, K.; Gerischer, S.; Slobinsky, D.; Perry, R. S. Dirac strings and magnetic monopoles in the spin ice $Dy_2Ti_2O_7$. *Science* **2009**, *326*, No. 411.

(5) Fennell, T.; Deen, P. P.; Wildes, A. R.; Schmalzl, K.; Prabhakaran, D.; Boothroyd, A. T.; Aldus, R. J.; McMorrow, D. F.; Bramwell, S. T. Magnetic coulomb phase in the spin ice $Ho_2Ti_2O_7$. *Science* **2009**, *326*, No. 415.

(6) Balents, L. Spin liquids in frustrated magnets. *Nature* **2010**, *464*, No. 199.

(7) Thompson, J. D.; McClarty, P. A.; Rønnow, H. M.; Regnault, L. P.; Sorge, A.; Gingras, M. J. P. Rods of neutron scattering intensity in $Yb_2Ti_2O_7$: compelling evidence for significant anisotropic exchange in a magnetic pyrochlore oxide. *Phys. Rev. Lett.* **2011**, *106*, No. 187202.

(8) Ramirez, A. P.; Hayashi, A.; Cava, R. J.; Siddharthan, R.; Shastry, B. S. Zero-point entropy in spin ice. *Nature* **1999**, *399*, 333−335.

(9) Chang, L. J.; Onoda, S.; Su, Y.; Kao, Y. J.; Tsuei, K. D.; Yasui, Y.; Kakurai, K.; Lees, M. R. Higgs transition from a magnetic Coulomb liquid to a ferromagnet in $Yb_2Ti_2O_7$. *Nat. Commun.* **2012**, *3*, No. 992.

(10) Applegate, R.; Hayre, N. R.; Singh, R. R. P.; Lin, T.; Day, A. G. R.; Gingras, M. J. P. Vindication of $Yb_2Ti_2O_7$ as a model exchange quantum spin ice. *Phys. Rev. Lett.* **2012**, *109*, No. 097205.

(11) Hayre, N. R.; Ross, K. A.; Applegate, R.; Lin, T.; Singh, R. R. P.; Gaulin, B. D.; Gingras, M. J. P. Thermodynamic properties of $Yb_2Ti_2O_7$ pyrochlore as a function of temperature and magnetic field: Validation of a quantum spin ice exchange Hamiltonian. *Phys. Rev. B* **2013**, *87*, No. 184423.

(12) Yasui, Y.; Soda, M.; Iikubo, S.; Ito, M.; Sato, M.; Hamaguchi, N.; Matsushita, T.; Wada, N.; Takeuchi, T.; Aso, N.; Kakurai, K. Ferromagnetic transition of pyrochlore compound $Yb_2Ti_2O_7$. *J. Phys. Soc. Jpn.* **2003**, *72*, No. 3014.

(13) Hodges, J. A.; Bonville, P.; Forget, A.; Yaouanc, A.; Dalmas de R'eotier, P.; Andr'e, G.; Rams, M.; Kr'olas, K.; Ritter, C.; Grubbens, P. C. M.; Kaiser, C. T.; King, P. J. C.; Baines, C. First-order transition in the spin dynamics of geometrically frustrated $Yb_2Ti_2O_7$. *Phys.Rev. Lett.* **2002**, *88*, No. 077204.

(14) Ross, K. A.; Ruff, J. P. C.; Adams, C. P.; Gardner, J. S.; Dabkowska, H. A.; Qiu, Y.; Copley, J. R. D.; Gaulin, B. D. Two-dimensional kagome correlations and field induced order in the ferromagnetic *XY* pyrochlore $Yb_2Ti_2O_7$. *Phys. Rev. Lett.* **2009**, *103*, No. 227202.

(15) Ross, K. A.; Yaraskavitch, L. R.; Laver, M.; Gardner, J. S.; Quilliam, J. A.; Meng, S.; Kycia, J. B.; Singh, D. K.; Proffen, Th.; Dabkowska, H. A.; Gaulin, B. D. Dimensional evolution of spin correlations in the magnetic pyrochlore $Yb_2Ti_2O_7$. *Phys. Rev. B* **2011**, *84*, No. 174442.

(16) Wong, A. W. C.; Hao, Z.; Gingras, M. J. P. Ground state phase diagram of generic *XY* pyrochlore magnets with quantum fluctuations. *Phys. Rev. B* **2013**, *88*, No. 144402.

(17) Ross, K. A.; Savary, L.; Gaulin, B. D.; Balents, L. Quantum excitations in quantum spin ice. *Phys. Rev. X* **2011**, *1*, No. 021002.

(18) Ross, A.; Proffen, Th.; Dabkowska, H. A.; Quilliam, J. A.; Yaraskavitch, L. R.; Kycia, J. B.; Gaulin, B. D. Lightly stuffed pyrochlore structure of single-crystalline $Yb_2Ti_2O_7$ grown by the optical floating zone technique. *Phys. Rev. B* **2012**, *86*, No. 174424.

(19) Trump, B. A.; Koohpayeh, S. M.; Livi, K. J. T.; Wen, J. J.; Arpino, K. E.; Ramasse, Q. M.; Brydson, R.; Feygenson, M.; Takeda, H.; Takigawa, M.; Kimura, K.; Nakatsuji, S.; Broholm, C. L.; McQueen, T. M. Universal geometric frustration in pyrochlores. *Nat. Commun.* **2018**, *9*, No. 2619.

(20) Dong, X. W.; Wang, K. F.; Luo, S. J.; Wan, J. G.; Liu, J. M. Coexistence of magnetic and ferroelectric behaviors of pyrochlore $Ho_2Ti_2O_7$. *J. Appl. Phys.* **2009**, *106*, No. 104101.

(21) Lin, L.; Xie, Y. L.; Wen, J. J.; Dong, S.; Yan, Z. B.; Liu, J. M. Experimental observation of magnetoelectricity in spin ice $Dy_2Ti_2O_7$. *J. M. New J. Phys.* **2015**, *17*, No. 123018.

(22) Liu, D.; Lin, L.; Liu, M. F.; Yan, Z. B.; Dong, S.; Liu, J. M. Multiferroicity in spin ice $Ho_2Ti_2O_7$: An investigation on single crystals. *J. Appl. Phys.* **2013**, *113*, No. 17D901.

(23) Saito, M.; Higashinaka, R.; Yoshiteru, M. Magnetodielectric response of the spin-ice $Dy_2Ti_2O_7$. *Phys. Rev. B* **2005**, *72*, No. 144422.

(24) Christopher, G.; Turner, J.; Roberto, E. E.; Juan, C. N. Dielectric Properties and relaxation of $Bi_2Ti_2O_7$. *J. Am. Ceram. Soc.* **2014**, *97*, 1763−1768.

(25) Salamat, A.; Hector, A. L.; McMillan, P. F.; Ritter, C. Structure, bonding, and phase relations in $Bi_2Sn_2O_7$ and $Bi_2Ti_2O_7$ pyrochlores: new insights from high pressure and high temperature studies. *Inorg. Chem.* **2011**, *50*, 11905−11913.

(26) Ewing, R. C.; Weber, W. J.; Lian, J. Nuclear waste disposal-pyrochlore ($A_2B_2O_7$): Nuclear waste form for the immobilization of plutonium and 'minor'' actinides. *J. Appl. Phys.* **2004**, *95*, No. 5949.

(27) Snyder, J.; Slusky, J. S.; Cava, R. J.; Schiffer, P. Dirty spin ice: The effect of dilution on spin freezing in $Dy_2Ti_2O_7$. *Phys. Rev. B* **2002**, *66*, No. 064432.

(28) Ubic, R.; Reaney, I. M. Structure and dielectric properties of lead pyrochlores. *J. Am. Ceram. Soc.* **2010**, *85*, 2472−2478.

(29) Ubic, R.; Reaney, I. M. Electron microscopy of lead pyroniobate. *J. Eur. Ceram. Soc.* **2001**, *21*, 2123−2126.

(30) Arpino, K. E.; Trump, B. A.; Scheie, A. O.; McQueen, T. M.; Koohpayehx, S. M. Impact of stoichiometry of $Yb_2Ti_2O_7$ on its physical properties. *Phys. Rev. B* **2017**, *95*, No. 094407.

(31) Kong, L.; Karatchevtseva, I.; Zhang, Y. A new method for production of glass-$Ln_2Ti_2O_7$ pyrochlore (Ln = Gd, Tb, Er, Yb). *J. Eur. Ceram. Soc.* **2017**, *37*, 4963−4972.

(32) Vandenborre, M. T.; Husson, E. Comparison of the force field in various pyrochlore families. I. the $A_2B_2O_7$ oxides. *J. Solid State Chem.* **1983**, *50*, 362−371.

(33) Vandenborre, M. T.; Husson, E.; Chatry, J. P.; Michel, D. Rare-earth titanates and stannates of pyrochlore structure; vibrational spectra and force fields. *J. Raman Spectrosc.* **1983**, *14*, 63−71.

(34) Mishra, A. K.; Poswal, H. K.; Sharma, S. M. The study of pressure induced structural phase transition in spin-frustrated $Yb_2Ti_2O_7$ pyrochlore. *J. Appl. Phys.* **2012**, *111*, No. 033509.

(35) Fu, Y.; Shan, Y.; Zhou, G.; Long, L. Y.; Wang, L. L.; Yin, K. B.; Guo, J. H.; Shen, J. C.; Liu, L. Z.; Wu, X. L. Electric strain in dual metal janus nanosheets induces structural phase transition for efficient hydrogen evolution. *Joule* **2019**, *3*, 2955−2967.

(36) Fang, D. W.; Tsung, C. W.; Xiao, R. L. Epitaxial stabilization of (111)-oriented frustrated quantum pyrochlore thin films. *J. Appl. Phys.* **2021**, *129*, No. 025302.

(37) Gao, L. S.; Zhang, S. N.; Zou, X. X.; Wang, J. F.; Su, J.; Chen, J. S. Oxygen vacancy engineering of titania-induced by Sr^{2+} dopants for visible-light-driven hydrogen evolution. *Inorg. Chem.* **2021**, *60*, 32−36.

(38) Yan, M. Y.; Yan, J. M.; Zhang, M. Y.; Chen, T. W.; Gao, G. Y.; Wang, F. F.; Chai, Y.; Zheng, R. K. Nonvolatile manipulation of electronic and ferromagnetic properties of NiO-Ni epitaxial film by ferroelectric polarization charge. *Appl. Phys. Lett.* **2020**, *117*, No. 232901.

(39) Liu, H.; Zou, Y. M.; Zhang, L.; Ling, L. S.; Yu, H. Y.; He, L.; Zhang, C. J.; Zhang, Y. H. Magnetic order and dynamical properties of the spin-frustrated magnet $Dy_{2-x}Yb_xTi_2O_7$. *J. Magn. Magn. Mater.* **2014**, *349*, 173−179.

(40) Giampaoli, G.; Li, J.; Ramirez, A. P.; Sleight, A. W.; Subramanian, M. A. $Bi_{2-x}Ca_xIr_2O_{6+y}$ pyrochlore phases: structure and properties with varied Ir oxidation state from 3.9+ to 4.3+. *Inorg. Chem.* **2017**, *56*, 4706−4715.

(41) Hodges, J. A.; Bonville, P.; Forget, A.; Rams, M.; Krolas, K.; Dhalenne, G. The crystal field and exchange interactions in $Yb_2Ti_2O_7$. *J. Phys.: Condens. Matter* **2001**, *13*, 9301−9310.

(42) Bramwell, S. T.; Field, M. N.; Harris, M. J.; Parkin, I. P. Bulk magnetization of the heavy rare earth titanate pyrochlores-a series of model frustrated magnets. *J. Phys.: Condens. Matter* **2000**, *12*, 483−495.

(43) Bogolubskiy, A. S.; Klepikova, A. S.; Rinkevich, A. B.; Neverov, V. N.; Nemytova, O. V.; Koroleva, M. S.; Piir, I. V.; Perov, D. V. Dielectric and magnetic properties of holmium and ytterbium titanates. *Low Temp. Phys.* **2021**, *47*, No. 79.

(44) He, X. J.; Li, L.; Xie, Z. S.; Zhang, Y. C.; Zhang, J.; Gu, Z. B.; Zhang, H. B.; Yuan, G. l.; Zhang, S. T. Composition-dependent electrical property of $(1-x)Sr_{0.75}Ba_{0.25}Nb_2O_6$-$xPbZr_{0.52}Ti_{0.48}O_3$ solid solution ceramics. *J. Eur. Ceram. Soc.* **2021**, *41*, 2435−2442.

(45) Pramod, K. Y.; Martin, T.; Chandan, U. Dielectric relaxations in $Ho_2Ti_2O_7$ and $Dy_2Ti_2O_7$ pyrochlores. *J. Phys. Chem. Solids* **2019**, *134*, 201−208.

(46) Du, H.; Wang, H.; Yao, X. Observations on structural evolution and dielectric properties of oxygen-deficient pyrochlores. *Ceram. Int.* **2004**, *30*, 1383−1387.

(47) Nino, J. C.; Lanagan, M. T.; Randall, C. A.; Kamba, S. Correlation between infrared phonon modes and dielectric relaxation in Bi_2O_3-ZnO-Nb_2O_5 cubic pyrochlore. *Appl. Phys. Lett.* **2002**, *81*, 4404−4406.

(48) Kamba, S.; Porokhonskyy, V.; Pashkin, A.; Bovtun, V.; Petzelt, J.; Nino, J. C.; Trolier, M. S.; Lanagan, M. T.; Randall, C. A. Anomalous broad dielectric relaxation in $Bi_{1.5}Zn_{1.0}Nb_{1.5}O_7$ pyrochlore. *Phys. Rev. B* **2002**, *66*, No. 054106.